

Applications of the simplified nozzle flow theory in model rocketry:

What is the effect of changing the nozzle divergence angle on the rocket engine performance and is there an optimum angle?

Extended Essay
Physics
Lauri Wirola
D-0678-030
Session May 2000
13th December 1999
Word count: 3981

Abstract

The physical size and mass of the nozzle, which are of a great interest to an amateur rocketist with a limited power output in rocket engines, are greatly affected by the divergence angle of the nozzle. However, the angle affects the thrust developed by the engine as well. Therefore, this research was set to examine *what the effect of changing the nozzle divergence angle on the rocket engine performance is and if there is an optimum angle.*

A simplified theory of a flow in a nozzle is introduced in order to be able to form a hypothesis and analyze the results obtained. A set of nozzles with equal expansion ratios of 16 and varying divergence angles were tested. Individual angles included 5, 10, 15, 20, 30 and 45 degrees. Actual rockets using potassiumnitrate-sucrose propellant were used in the experiments in order to provide real circumstances for nozzles. Two sets of rockets were launched.

Thrusts generated by different nozzles were measured by the pressure developed by the piston, on which the engine exerted thrust in a stationary test bench. The thrusts are analyzed by calculating a specific impulse developed by each engine and comparing these. Two distinct methods, which showed to provide results in accordance with each other, of calculating the specific impulse are introduced due to the complexity of the thrust curves.

The experiments showed a notable variation in thrust depending upon the divergence angle and showed the 15°-nozzle to be the best of the tested set. Furthermore, the tendencies can be explained by the assumptions made in the flow theories. The experiments also showed that the thrust developed by the nearest 20°-nozzle is such that the reduction of weight achieved by the use of a larger divergence angle will not compensate for the substantial decrease in the thrust.

Tiivistelmä

Rakettiharrastajien ikuinen ongelma on saada rakettiensa massa mahdollisimman pieneksi. Rakettisuuttimet, jotka useimmiten valmistetaan metallista, ovat rakettimoottoreiden painavimpia yksittäisiä osia. Suuttimella on kuitenkin merkittävä rooli moottorin tuottaman työnnön maksimoinnissa, mistä syystä suuttimilla on tarkasti määritetty muoto ja rakenne. Suuttimen koon optimoinnilla onkin suuri merkitys moottorin laukaisumassaa ajatellen.

Tutkimuksessa haetaan vastausta kysymykseen, mikä on suuttimen aukenevan osan aukenemiskulman vaikutus rakettimoottorin kehittämään työntöön, ja onko suuttimella mahdollisesti optimiaukeamiskulmaa. Hypoteesia etsitään yksinkertaistettujen virtausmallien avulla, joita verrataan saatuihin tuloksiin. Sarja suuttimia, joiden laajenemiskerroin on 16 valmistettiin 5, 10, 15, 20, 30 and 45 -asteisilla kulmissilla. Kokeissa käytettiin aitoja rakettimoottoreita, joiden polttoaineena oli kaliumnitraatti-sokeri seos. Kokeissa käytettiin kahta rakettisarjaa.

Moottoreita testattiin kiinteässä testilaitteessa, jossa moottori työntää sylinderissä mäntää vasten ja kehittää näin paineen, jota mitataan. Mittaustuloksista laskettiin jokaiselle suuttimelle ominaisimpulssit, joita vertaillaan. Työntökäyrien hankalista muodoista johtuen, käytettiin kahta erilaista laskentatapaa, jotka kuitenkin osoittivat samansuuntaisia tuloksia.

Mittaustulokset osoittavat selkeästi, että suuttimen aukeamiskulmalla on suuri merkitys työnnön kannalta. Tulokset näyttivät 15-asteisen suuttimen tuottavan selkeästi parhaan työnnön. Tuloksia vertaillessa huomattiin myös, että käytettäessä 20-asteista suutinta, työntö on niin paljon heikompi, ettei suuremman aukeamiskulman tarjoama pienempi massa pysty tätä kompensoimaan. Pohdittaessa kuitenkin virtausteorioiden olettamuksia, huomataan, että havaitut työnnöt pystytään näiden pohjalta kvalitatiivisesti selittämään. Toisessa rakettisarjassa käytetty heikompilaatuinen polttoaine kasvatti huomattavasti eroja työnnöissä eri aukeamiskulmien välillä.

"We choose to go to the moon. We choose to go to the moon in this decade and do the other things, not because they are easy, but because they are hard, because that goal will serve to organize and measure the best of our energies and skills, because that challenge is one that we are willing to accept, one we are unwilling to postpone, and one which we intend to win, and the others, too."

John F. Kennedy, 1962

Table of contents

List of figures	4
-----------------	---

List of tables	4
List of graphs	4
1. Introduction	5
2. Nozzle flow theory	5
2.1 Simplifications and assumptions behind the isentropic flow theory	5
2.2 Nozzle properties and theory	7
2.3 Divergence angle	9
2.4 Experiments	9
3. Test engines	11
3.1 Structure of the engines	11
3.2 Safety issues	11
4. Measurements	12
4.1 Measurement equipment	12
4.2 Method for the performance evaluation	13
4.3 Error sources	14
5. Results and data analysis	15
5.1 Individual analysis of the sets	15
5.2 Averaged analysis	17
6. Conclusion	20
Bibliography	21
Acknowledgements	21
Appendix A	
Appendix B	
Appendix C	
Appendix D	

1. Introduction

Ever since the conclusive steps taken by nazis during World War II with the development of their V2-rocket and the culmination of the space race in 1961 with cosmonaut Juri Gagarin's flight and astronaut Neil Armstrong's moon walk in 1969, rocketry has also inspired amateur rocket scientists.

The model rockets built by enthusiasts are in fact often authentic scaled copies of their real world exemplars.

Nozzle design is essential in model rocketry as the thrust generated by the rocket engine can be increased manifold with an optimal nozzle. However, the research done with nozzles concentrates mainly on the nozzles used in space vehicles or other applications. It is, however, vital to an enthusiast as well to obtain an efficient and small nozzle since also the mass issue must be taken into account.

Nozzles first narrowing and then widening are familiar from variety of applications. In the theory section it will be shown why the shape must be so. Therefore, one method of reducing the size and mass of the nozzle is to increase the angle of widening. A closer look at the theory behind nozzles will give a more specific view on what problems can be expected to occur as the angle is varied.

This research is set to examine the relationship between the divergence angle of the nozzle and the engine performance as well as to seek for the optimum angle. The objectives set for the research are first to develop a method for the performance analysis and secondly empirically examine various divergence angles and evaluate the capabilities of the examined nozzles.

2. Nozzle flow theory

2.1 Simplifications and assumptions behind the isentropic flow theory

Derivations of the formulae will not be presented in this paper since they are available in the references given. However, general assumptions of the nozzle flow theory will be discussed in detail in order to be able to compare the theoretical predictions with measured values.

The fundamental equations forming the basis of the nozzle flow theory are

1. *Continuity of flow* stating the mass of flow flowing through any given cross-section is constant
2. *First law of thermodynamics* claiming the conservation of energy
3. *Equation of state*, which includes the ideal gas law

4. *Second law of thermodynamics*
5. *Conservation of momentum*
6. *Process equation*

$$\frac{P}{\rho^\gamma} = \text{constant} \text{, where } P = \text{pressure}$$

ρ = density

$$\gamma = \frac{C_p}{C_v}, \text{ where } C_p = \text{heat capacity in constant pressure}$$

C_v = heat capacity in constant volume

Assumptions on the flow included in the theory contain

1. The flow is one-dimensional and steady.

In one-dimensional flow the fluid properties (velocity, pressure, density) do not vary across a given cross-section in time. Properties vary from one cross-section to another, but remain constant for a given plane. Steady flow also assumes that the cross-section does not change rapidly.

2. The flow is isentropic.

Isentropic flow is an ideal flow in which no frictional or heat losses occur. Enthalpy of the gas is converted to kinetic energy as required of an accelerating flow.

3. No chemical reactions take place in the nozzle flow and gas is homogenous.

This is required to satisfy the condition that no heat addition is made during the flow in the nozzle. Homogeneity arises from the fact that flow is assumed to consist of ideal gas and therefore no solid material should occur in the flow.

5. There are no shock waves.

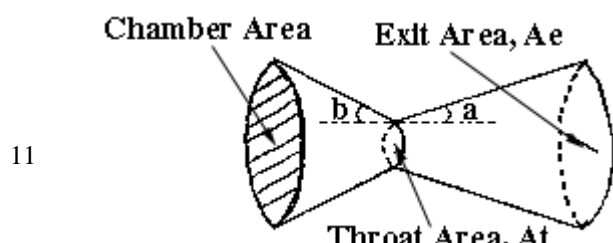
Occurrence of shock waves will lead to energy losses and entropy increases within the flow.

6. The rocket is not accelerating.

In the experiments a non-accelerating situation will be achieved as the engine is inserted in a stationary test bench.

2.2 Nozzle properties and theory

The function of the nozzle is to accelerate gases produced by the propellant to maximum velocity in order to obtain



maximum thrust. In *deLaval nozzles* first converging and then diverging, acceleration is obtained by varying the cross-sectional area of the nozzle (figure 1.).

From the presumptions introduced above, it can be deduced that velocity of the flow and the area are dependent by

$$\frac{dA}{A} = -\frac{dv}{v} \cdot (1 - M^2), \text{ where } A = \text{Area of the nozzle cross section}$$

v = velocity of the flow

$$M = \text{local mach number} = \frac{\text{velocity}}{\text{local velocity of sound}}$$

From the equation it can be observed that accelerating the flow from rest in the chamber requires a converging segment in the nozzle. Initially the flow is subsonic and mach number is below one, and therefore negative dA/A is needed for an accelerating flow and the nozzle is converging. Consequently, the flow achieves the velocity of sound. At this point $dA/A = 0$ and hence the area of the nozzle passes through the minimum or maximum point. However, as the velocity of the flow crosses unity, dA/A and dv/v have the same sign by the equation. Therefore, now the area of the nozzle increases simultaneously with the flow velocity. Hence, the point at which $dA/A = 0$ must be a minimum and it can be concluded that the nozzle area must pass through a minimum in order for flow to obtain large exit velocity [1]. The dependence of mach number upon the ratio of the cross-sectional and the throat area is given [3] by

$$\frac{A}{A_t} = \frac{1}{M} \cdot \left[\frac{1 + \frac{\gamma - 1}{2} \cdot M^2}{\frac{\gamma + 1}{2}} \right]^{\frac{\gamma + 1}{2(\gamma - 1)}}$$

, where A = Area of the nozzle cross section

A_t = Throat area of the nozzle

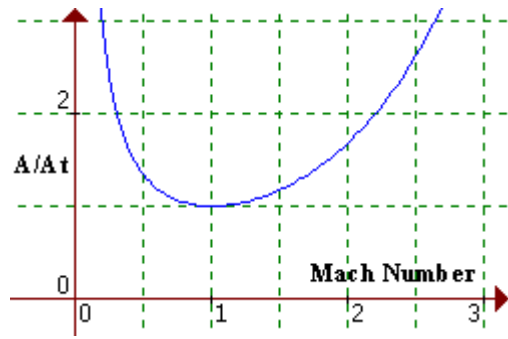


Figure 2. Area ratio as a function of local mach number for $\gamma = 1,4$.

of which graph (figure 2.) further explains the shape of the nozzle.

Then, the exit area of the nozzle clearly has an effect on the thrust developed. It can be shown that

$$F = A_t \cdot P_c \cdot \sqrt{\frac{2\gamma^2}{\gamma-1} \cdot \left(\frac{2}{\gamma+1}\right)^{\frac{\gamma+1}{\gamma-1}} \cdot \left(1 - \left(\frac{P_e}{P_c}\right)^{\frac{\gamma-1}{\gamma}}\right)} + (P_e - P_a)A_e$$

$$\frac{A_t}{A_e} = \frac{1}{\varepsilon} = \left(\frac{\gamma+1}{2}\right)^{\frac{1}{\gamma-1}} \cdot \left(\frac{P_e}{P_c}\right)^{\frac{1}{\gamma}} \cdot \sqrt{\frac{\gamma+1}{\gamma-1} \cdot \left(1 - \left(\frac{P_e}{P_c}\right)^{\frac{\gamma-1}{\gamma}}\right)}$$

, where F = thrust developed by the engine

A_t = throat area

A_e = exit area

P_c = chamber pressure

P_e = exit pressure

P_a = atmospheric pressure

ε = expansion ratio

The first equation shows how the thrust developed by the nozzle is dependent upon the exit pressure of the gas flow. However, the second equation shows how the exit pressure is dependent upon the *expansion ratio*, ε , the ratio of the exit area to the throat area. The expansion ratios commonly lie between 2 and 16.

It should also be acknowledged that the maximum thrust is achieved as the exit pressure equals to the atmospheric pressure. This is the design condition for a nozzle and no shock waves occur in the flow at this expansion ratio.

2.3 Divergence angle

The flow theory used to explain the thrust resulting from varying the expansion ratio does not consider how steeply the area changes in the nozzle. However, the angle determines the physical size of the nozzle for the given expansion ratio. Therefore, the greater the angle could be, more beneficial it would be considering the payload of the rocket.

Now, as the increase in the angle is considered, the basic function of the nozzle to curtail the sidewise expansion of the gas to ensure the maximum velocity vector of the particles parallel to the

rocket, must be borne in mind [5]. Great angles will allow for considerable amount of sidewise motion reducing thrust. Now, the aim set for the research is to determine, what is the magnitude of the thrust loss as the divergence angle, α , is increased.

A simple method for approximating the thrust loss due to the momentum dispersion of the gas particles is the magnitude of a λ -factor given [6] by

$$\lambda = \frac{1}{2}(1 + \cos \alpha)$$

and

$$F_{\text{effective}} = \lambda \cdot F_{\text{theoretical}}$$

The figure $1-\lambda$ is therefore fraction of the theoretical thrust lost because of the divergence of the nozzle.

2.4 Experiments

The theories introduced above yield that for a given expansion ratio the theoretical thrust is constant whatever the divergence angle taking into account only the simplified flow theory and as the momentum dispersion is acknowledged, larger divergence angles will result in thrust losses. Therefore, in the experiments the expansion ratio will be kept constant at $\varepsilon = 16$ and six different divergence angles will be researched in order to determine whether a compromise can be made with the angle as using infinitely long nozzles with small divergence angles is not possible due to the mass question.

The experiment matrix is as follows

$\varepsilon = 16$		
$\alpha / {}^\circ$	λ	Performance*
5	0,998	
10	0,992	
15	0,983	
20	0,970	
30	0,933	

45	0,854	
----	-------	--

Table 1. The experiment matrix
* = the performance analysis
method will be discussed later

The nozzles were lathed in a round solid iron rod of a diameter of 16 mm.

Two sets of rockets, sets A and B, will be launched, which results in a fairly small sample space. However, building rockets is time consuming and expensive and therefore there are no resources to build a greater experiment matrix.

3. Test engines

3.1 Structure of the engines

The type of rocket engine used is shown in the figure 3. beside. The body of the engine is manufactured of PVC-pipe with an inside diameter of 16 mm. The top has been sealed with ceramic glue in order to prevent pressure losses as well as deformation resulting from heat.

Potassiumnitrate-Sucrose propellant, KN-Sucrose, was chosen as the propellant. It consist 65% of potassium nitrate, KNO_3 , and 35% of sucrose. The important characteristics of KN-Sucrose are its burning temperature, 1800 K, and γ of its decomposition gases, 1,4. The propellant is melted liquid in approximately 470 K and casted into the rocket body. Approximately 25 grams of propellant is used in each engine, but the exact amount is determined by the difference in weight as empty and filled.

The casting is required in order to produce homogenous and bubble free propellant grains and to ensure similar test conditions for each nozzle. Amateur rockets using solid propellants are core-burners, in which the burning area of the propellant is artificially increased by the hollow propellant grain in order to increase burning rate. The engine used has a core of 5 mm. The nozzles are attached to the rocket body by pinching.

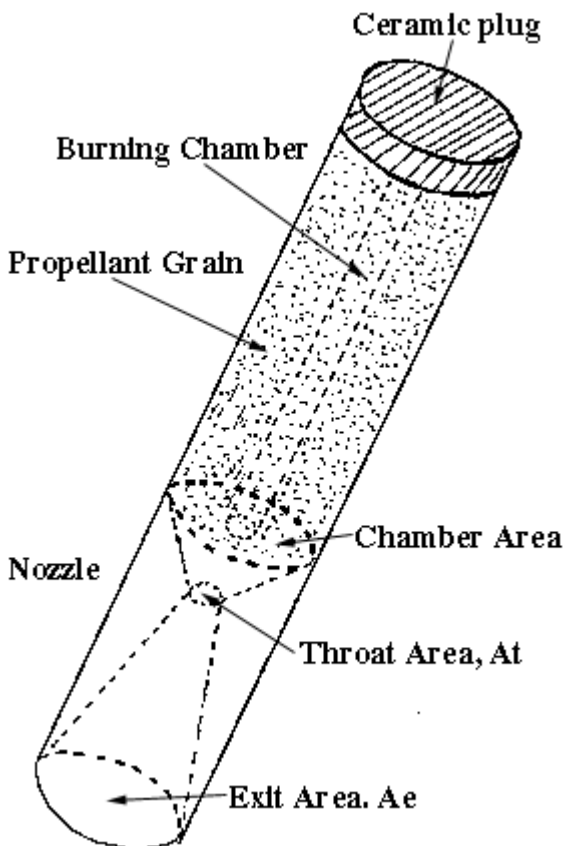


Figure 3. The engine structure. Actual image of an engine used can be found in Appendix D.

3.2 Safety issues

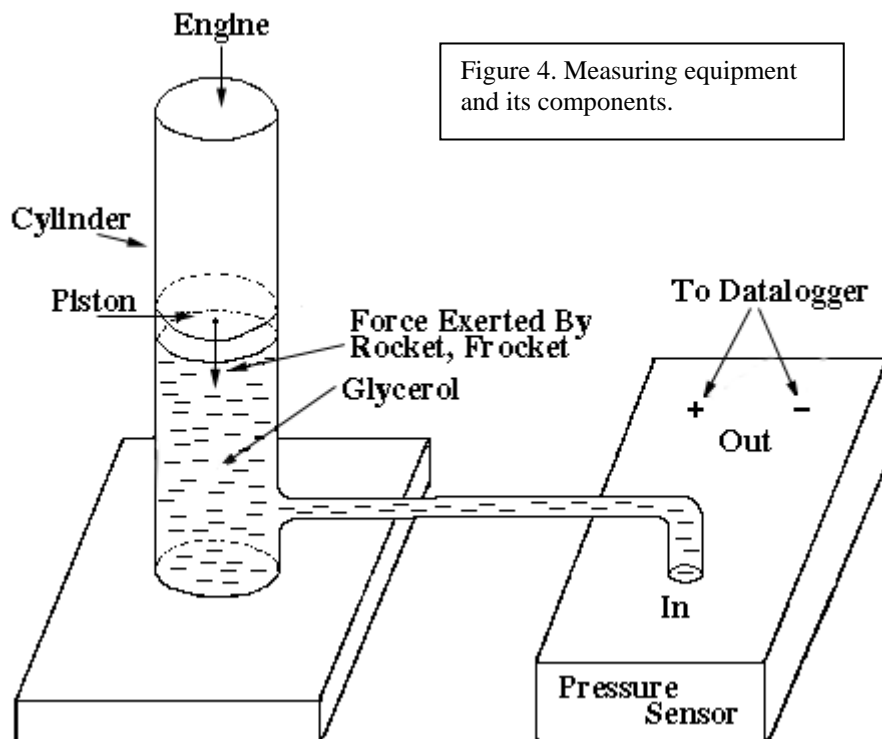
Rocket engines are not safe to operate with without prior knowledge and experience in amateur rocketing. The propellant casting is the most critical step and must be performed with fast availability of extinguishing equipment. Adequate measures must also be taken in protecting oneself with a mask and clothes of anti-flammable material. The risk of minor burns is also great due to handling of heated liquid materials. On the other hand, the propellant is relatively safe to handle as it is not readily ignited by friction and has a high flash temperature, over 650 K. Another advantage of KN-Sucrose is that it is completely non-toxic.

Plastic is used as the body material due to its flexibility. Should there be overpressure, the body will not break into pieces, but splits and discharges the pressure and therefore no explosion will occur. The measurement equipment are adequately protected to prevent contact with hot discharging gases. To further increase safety, ignition is performed electrically, which allows for an exact ignition timing. In addition, the measurement equipment is automated so that the recording starts automatically immediately as force is applied by the engine on the sensor.

4. Measurements

4.1 Measurement equipment

The method chosen for measuring the thrust developed by the engine was by measuring the pressure. A simplified model of the equipment used is shown below (figure 4.). An actual image of the system can be found in appendix D.



Equipment consists of a vertical piston filled with glycerol. The engine with a specific nozzle will be set on the piston vertically as well and the pressure under the piston is led via a tube to a pressure sensor. The pressure sensor provides a voltage linearly dependent upon the applied pressure and a datalogger will record the voltage level every 30 ms.

In the vertical position of the piston, the mass of the engine and nozzle itself will apply force on the piston. Should the system be inserted horizontally such a problem would not occur. However, in this case the torque applied by the rocket will add an uncertainty factor. The heaviest segment of the rocket, the nozzle, must be exposed to air to ensure sufficient cooling, which provides the nozzle mass a moment arm and forces some parts of the engine against the cylinder walls causing friction. This problem is mostly solved by inserting the piston in an upright position. However, the mass of the engine is reducing constantly during the burning. Now, by assuming that the rate of burning is constant for each rocket-nozzle combination, which is a reasonable assumption, this factor may be neglected as being a similar systematic error for each experiment.

4.2 Method for the performance evaluation

The performance of an engine is often described by the specific impulse, I_{sp} , given by the engine, which is defined as the impulse given per unit mass of propellant. The total impulse given by the engine is by definition the area under the force-time graph. Hence,

$$I_{sp} = \frac{\int F(t) dt}{m_{prop}} , \quad [I_{sp}] = \frac{[F] \cdot [t]}{[m]} = \frac{Ns}{kg}$$

Now, as discussed, the measurement equipment is designed to measure the pressure in the liquid. This pressure is defined in terms of the force applied by the rocket, F_{rocket} , and the area of the piston, A_{piston} , by

$$P = \frac{F_{rocket}}{A_{piston}} \Leftrightarrow F_{rocket} = A_{piston} \cdot P$$

Therefore, F_{rocket} is linearly proportional to P . However, the voltage output of the sensor is also directly proportional to P and hence it can be concluded that the voltage output and F_{rocket} correlate linearly as well.

Thus, the area under the voltage-time curve is directly proportional to the total impulse developed. The software used to analyze the data recorded is capable of determining this area to great accuracy. Furthermore, this area divided by the mass of the propellant results in a figure proportional to the specific impulse. The figure obtained is then divided by the maximum figure and multiplied by 100

to highlight differences and so the maximum index number is 100. Moreover, because of the division by maximum, the index is dimensionless. Therefore, a concept of *specific impulse index*, I_{index} , is introduced, which now provides a simple method to compare the relative performances. Hence,

$$I_{\text{index}} = \frac{\int V(t) dt}{m_{\text{prop}}} \cdot \frac{100}{I_{\text{sp}}(\text{max})}$$

The figure 5. shows a typical thrust curve produced by a rocket engine. By looking at the graph, it is clear that problems do occur in deciding to which point to integrate. Therefore, two different methods will be utilized.

Index A is based on finding the area under the curve from the beginning of the thrust ($t=0$) to the point where the derivative of the curve is minimum. This point is shown as point A in the figure to which the vertical line dV/dt is a tangent. This point may be assumed to be the point at which efficient burning ends.

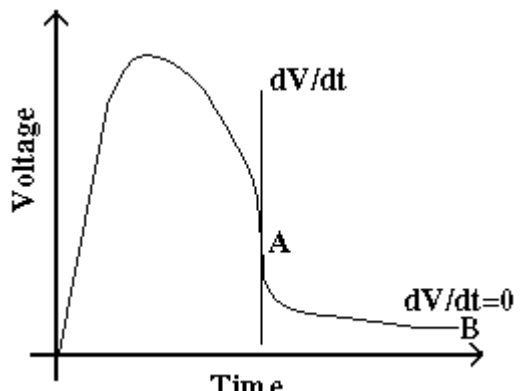


Figure 5. A typical thrust curve

Index B is based integrating the curve from the beginning ($t=0$) to the point at which dV/dt equals zero shown as point B in the figure. At this point all the burning has ceased. Voltage at that point may differ from zero because of the small friction in the piston due which the piston will not return exactly to equilibrium condition. This voltage, however, is small and does not have a significant effect on the results.

4.3 Error sources

The method of setting up the equipment introduced above aims at reducing friction. However, there will be friction involved in the piston itself. The piston must be built rigid enough to prevent the glycerol from leaking, but must also move smoothly. This is achieved by the use of lubricant as the fluid. Furthermore, expansion of the tube applying pressure on the sensor will be an error source. Considering the sensor itself, it must be noted that the sensor does not respond infinitely rapidly to changes in pressure. However, its resolution is enough for the used recording interval of 30 ms. Small error is added in the cables transferring data from the sensor to the logger due to their resistance.

5. Results and data analysis

5.1 Individual analysis of the sets

Individual thrust curves are presented in the appendix A.

Sets A and B refer to the two sets of engines launched.

"A" and "B" in brackets after " I_{sp} " and "Index" refer to different evaluation methods introduced. As the index values were calculated, sets A and B were considered as independent sets.

Set A (Table 2.)

The engine number 5 was lost due to structural failure in the engine.

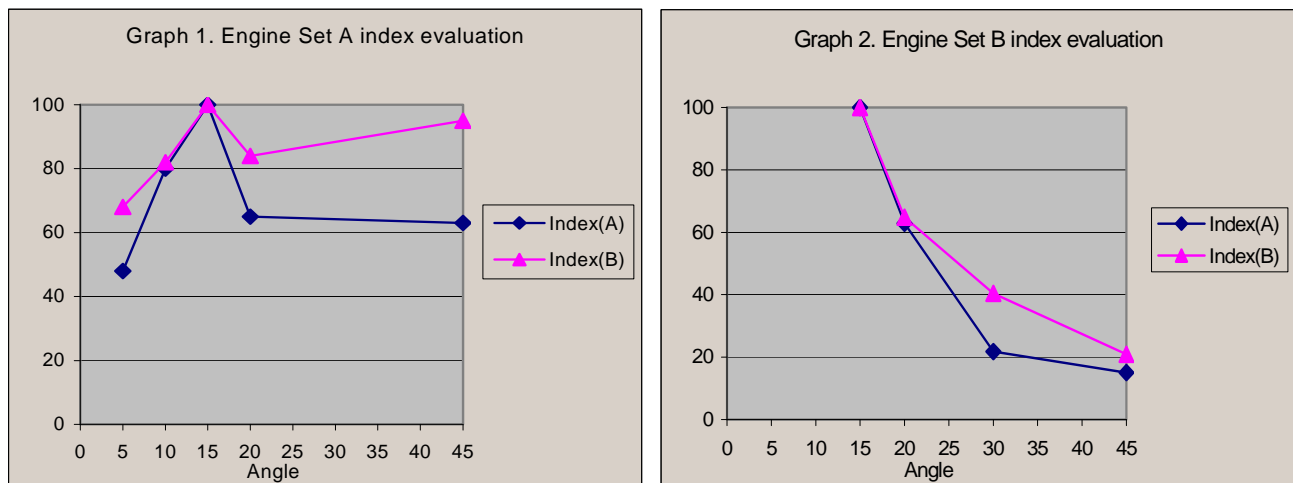
Engine	Angle $\alpha / {}^\circ$	$I_{sp} (A)$ $/ Vskg^{-1}$	$I_{sp} (B)$ $/ Vskg^{-1}$	Index(A)	Index(B)
1a	5	7,484	12,474	48	68
2a	10	12,479	14,975	80	82

3a	15	15,625	18,229	100	100
4a	20	10,195	15,293	65	84
5a	30				
6a	45	9,901	17,327	63	95

Set B (Table 3.)

The engines numbers 1 and 2 were lost due to structural failure in the engines.

Engine	Angle $\alpha / {}^\circ$	$I_{sp}(A) / Vskg^{-1}$	$I_{sp}(B) / Vskg^{-1}$	Index(A)	Index(B)
1b	5				
2b	10				
3b	15	36,466	39,271	100	100
4b	20	22,920	25,467	63	65
5b	30	7,937	15,873	22	40
6b	45	5,477	8,215	15	21



The graphs above show how the two evaluation methods correlate and give results in the same direction within the same set. Therefore, the nozzle structure not only affects the thrust developed during the maximum burn, but also has an effect after the maximum burn as measured by index B.

The both sets seem to imply that 15° is the most efficient nozzle. The λ -factor suggests 1,5% and 0,9% less thrust for 15° -nozzle than for 5° - and 10° -nozzles respectively. In the set A, for instance, the 5° -nozzle is measured to have 52% and 32% less thrust than the 15° -nozzle and the thrust drops are much greater than predicted. However, the isentropic flow theory, which predicts thrust to stay

constant whatever the divergence angle as long as the expansion ratio stays constant, included that no heat losses occur in the nozzle. It can be shown (Appendix C) that the 5°-nozzle has 3 times more area capable of transferring heat off during the flow process compared to the best nozzle. The same applies to the 10°-nozzle as well having 1,5 times the area of the 15°-nozzle.

It also seems that as 15° is exceeded the momentum dispersion due to greater divergence angle becomes significant and the thrust drops. The significant drop of thrust after 15° is confirmed by the set B. The 20°-nozzle is already approximately 35% more inefficient and the decline of thrust is markedly rapid in the set B as the angle increases (graph 2). However, as the 5°- and 10°-nozzles were lost in the set B, it cannot be said if the 15°-nozzle is the best of the tested nozzles by looking only at the set B.

The two sets seem, however, to contradict with the 45°-nozzle. In the set A, its thrust does not deviate significantly from the 15°-nozzle, but in the set B, the thrust is only 15-21% of the maximum thrust depending upon the evaluation method. The effect could be explained by the fact that the 45°-nozzle has a fourth of the area losing heat to the surroundings compared to the 15°-nozzle. However, by looking at the 20°-nozzles of the both sets, it can be seen that both confirm the decline in thrust as 15° is exceeded. Furthermore, by considering the set B, the reduction of the area by 37% from the 20°-nozzle to the 30°-nozzle still results in a significant drop of thrust. Therefore, it does not seem probable that a rapid rise in thrust should occur from 30° to 45° although the area drops again by 42%. By the λ -factor it may also be expected that the widest nozzle loses significantly in thrust because of the momentum dispersion, but also because the flow does not have time to settle to a steady state in the nozzle due to its small length and therefore energy is lost in turbulence. This drop is confirmed by the set B. A record for a 30°-nozzle in the set A might solve the contradiction. Therefore, further experimentation is needed in this area.

In the experiments it was observed that the propellant used in the set B was more inhomogeneous. Uneven burning of the propellant can also be seen in the thrust curves produced by the set B (Appendix A). Now, looking at the specific impulses for sets A and B in tables 2 and 3 shows how the absolute values deviate more strongly in the set B. Therefore, the significance of the nozzle structure seems to become more emphasized as optimal propellant is not used. This is most likely due to the increased amount of solid material in the flow and increased velocity lag of the solid particles. The occurrence of the *two-phase flow* [6], in which there are solid particles, may also account for the fact that λ -factor predicts such small losses compared to the measured values as it assumes an ideal flow of homogenous gas.

5.2 Averaged analysis

Further analysis is made by combining the two sets and considering them as one.

Averaged data (Table 4.)

The average propellant mass and area under the curve are used.

Engine	Angle $\alpha / {}^\circ$	M_{prop} / kg	Area (A) / Vs	Area (B) / Vs	I_{sp} (A) / $Vskg^{-1}$	I_{sp} (B) / $Vskg^{-1}$	Index(A)	Index(B)
1	5	0,0241	0,18	0,30	7,484	12,474	29	44
2	10	0,0240	0,30	0,36	12,479	14,975	49	53
3	15	0,0222	0,57	0,63	25,658	28,359	100	100
4	20	0,0236	0,39	0,48	16,561	20,382	65	72
5	30	0,0227	0,18	0,36	7,937	15,873	31	56
6	45	0,0231	0,18	0,30	7,801	13,001	30	46

Averaged indices (Table 5.)

The average values of the indices calculated for sets A and B separately are used.

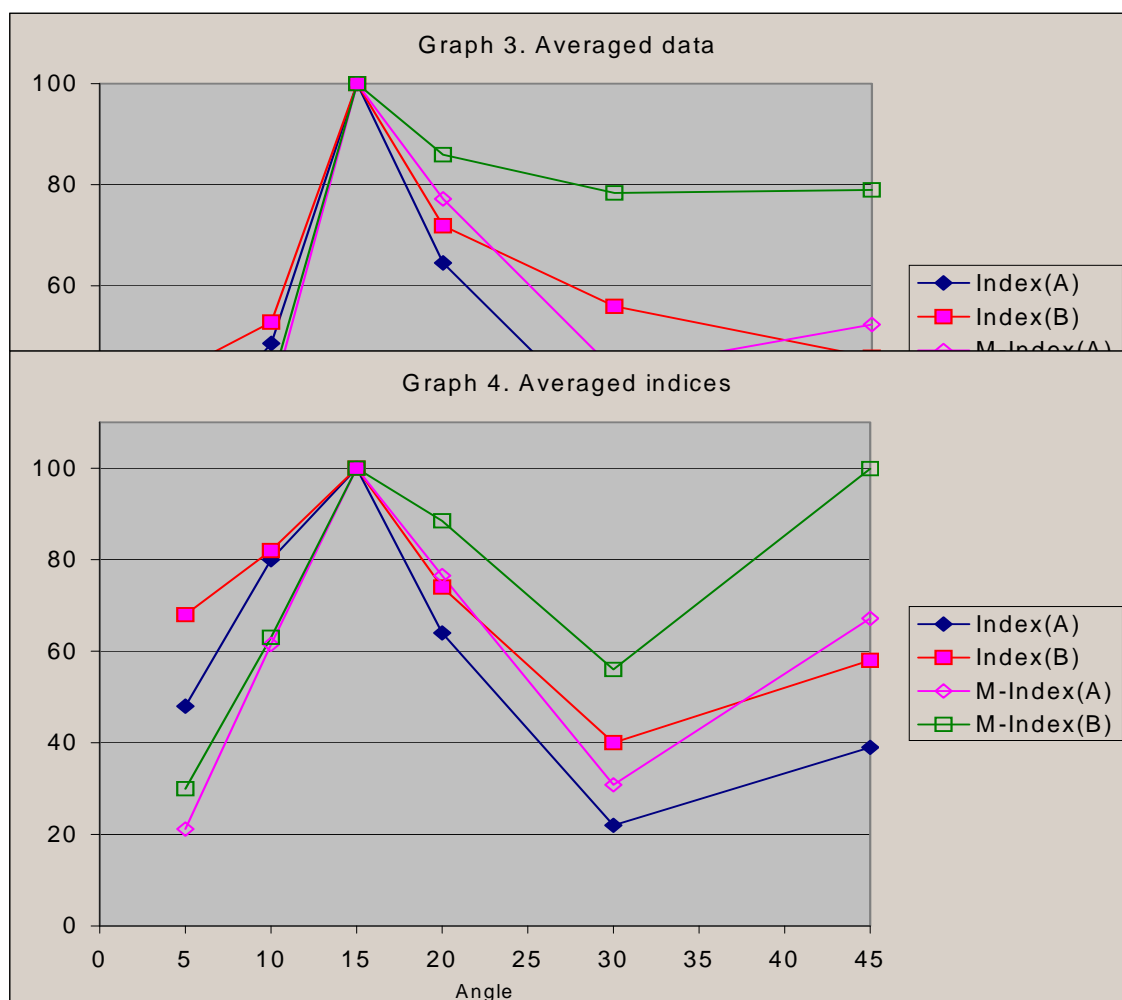
Engine	Angle $\alpha / {}^\circ$	Index(A)	Index(B)
1	5	48	68
2	10	80	82
3	15	100	100
4	20	64	74
5	30	22	40
6	45	39	58

Mass factors (Table 6.)

For the combined data, also mass corrected values are calculated. In the table 6 below, masses for individual nozzles used are given as well as relative masses to the most efficient, 15° , nozzle. Based on these M-index(A) and M-index(B) are calculated by dividing the index value A or B respectively by the mass factor in order to be able to contrast the nozzle masses to the results more efficiently.

Engine	Angle / °	Nozzle mass / kg	Relative mass	Averaged data		Averaged indices	
				M-index(A)	M-index(B)	M-index(A)	M-index(B)
1	5	0,0763	2,27	13	19	21	30
2	10	0,0437	1,30	37	41	62	63
3	15	0,0336	1,00	100	100	100	100
4	20	0,0281	0,84	77	86	77	89
5	30	0,0240	0,71	43	78	31	56
6	45	0,0195	0,58	52	79	67	100

M-index(A) and M-index(B) are shown alongside with the averaged data and indices in the following graphs.



Both averaging methods confirm the result of 15°-nozzle being the most efficient. Averaging the raw data gives somewhat greater weight to the strong results of the set B. In the set B, the 45°-nozzle is clearly the weakest one and thus drops the average value so that its performance is by index A equivalent to the 5°- and 30°-nozzles and by index B as inefficient as the 5°-nozzle. Averaging the index numbers give a similar weight to both sets and therefore the 45°-nozzle is seen to be more efficient than the 30°-nozzle. The index-method is more reliable compared to averaging the raw data, as it levels the differences between the sets arising from factors independent of the nozzles, such as propellant.

The thrust data corrected for the mass of the nozzle in M-index A and B confirm the fact that although the nozzles with angles greater than 15° have smaller masses, they are still not competitive against the 15°-nozzle. The correction gives somewhat better performance for the nozzles with larger angles than 15°, but with smaller angles the effect is opposite. Their weaknesses in both, performance and mass, are evident. However, considering the averaged indices data, it can be seen that mass correction increases the relative thrust of the 45°-nozzle to equal level with the 15°-nozzle. This further emphasizes the fact that the 45°-nozzle should be tested more, although it may occur that the high thrust measured is due to an error.

6. Conclusion

The isentropic nozzle flow theory is extensively being used amongst amateur circuits due to its simplicity to calculate expansion ratios and thrusts. The research was set to examine whether the divergence angle of the nozzle has an effect on the thrust. The estimates of the thrust drops given by λ -factor were noticed to be underestimates and much greater variation was observed. The results obtained seem to confirm the intuitive result established in amateur rocketry that the 15°-nozzle is the most efficient nozzle of the tested set. The closest nozzle, 20°, resulted in such a significant thrust reduction that the decrease in mass could not compensate for it, which is the case for all the other nozzle types experimented as well.

Further experimentation will, however, be needed to solve whether some divergence angle in the vicinity of 15° is even more efficient. However, this research has established an important narrowing of the angles to be tested in the next phase. For the purposes of further experimentation,

reliable testing equipment and data evaluation method have been developed. Painstaking efforts were taken to construct the piston system as frictionless as possible. This included building various prototypes before accepting the one used. Further problems were caused by cold weather and ultimately temperature dropping below zero during testing.

The research not only evoke a question whether a more efficient nozzle angle can be found, but also whether the same trend continues with other expansion ratios as well. $\varepsilon=16$ was used because of its general use in the small scale rocket engines as tested, but further testing might include testing with expansion ratios of 8 and 12 also commonly used.

Bibliography

- [1] Fox, Robert W., McDonald, Alan T., *Introduction to Fluid Mechanics, 2nd edition*, John Wiley & Sons Inc., New York 1978
- [2] Groves, G.V., *Dynamics of Rockets and Satellites*, North-Holland Publishing Company, Amsterdam 1965
- [3] Loh, W. H. T., *Jet, Rocket, Nuclear, Ion and Electric Propulsion Theory and Design*, Springer-Verlag New York Inc., 1968
- [4] Milligan, Timothy S. Van, *Model Rocket Design and Construction*, Kalmbach Publishing Co. 1995
- [5] Rosser, J. Barkley, Newton, Robert R., Gross, George L., *Mathematical Theory of Rocket Flight*, McGraw-Hill Book Company Inc., New York 1947
- [6] Timnat, Y.M., *Advanced Chemical Rocket Propulsion*, Academic Press Inc., London 1987

Acknowledgements

International Baccalaureate Organisation, Geneva
 This assignment has been done as a part of The International Baccalaureate Diploma Programme by candidate Lauri Wirola, D-0678-030, for the May 2000 session.

Hannu Wirola, Master of Science, civ. eng.
 For technical support in measuring techniques

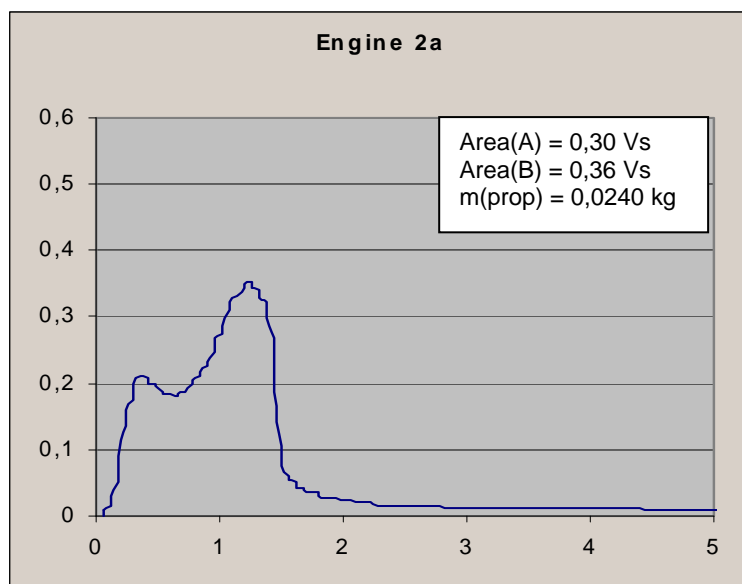
Richard Nakka, Mechanical Engineer
For providing background information

Torsti Tulenheimo, Economist, Mechanical Engineer
Fastems Oy Ab
For nozzle construction

Appendix B

Model calculation for the specific impulse index for the 10°-nozzle engine of the set A (Engine 2a).

The thrust curve for the engine 2a is given below.



The integration by the method A, yields for the area under the curve

$$\text{Area} = 0,30 \text{ Vs.}$$

The mass of the propellant used in the engine 2a is 0,0240 kg.

Therefore, the specific impulse is

$$I_{sp} = \frac{0,30 \text{ Vs}}{0,0240 \text{ kg}} = 12,5 \text{ Vs/kg}$$

The maximum specific impulse was obtained in the set A from the engine 3a, of which specific impulse, $I_{sp}(\max) = 15,625 \text{ Vs kg}^{-1}$.

Therefore, the specific impulse index by the method A for the engine 2a is

$$I_{index} = \frac{12,5 \text{ Vs/kg}}{15,625 \text{ Vs/kg}} \cdot 100 = 80$$

as indicated in the table 2.

Appendix C

Calculation method for comparing the outer areas of different nozzles.

The outer area of the nozzle capable of transferring heat to the surroundings is clearly dependent upon the divergence angle. It can be shown that the outer area of the diverging section of the nozzle having a divergence angle of α is approximately given by

$$A = \frac{2\pi r^2}{\tan \alpha}$$

, where r is the radius of the cylinder into which the nozzle shape is lathed.

Therefore, the area ratio of the nozzles having divergence angles of α_1 and α_2 is given by

$$\frac{A_1}{A_2} = \frac{\frac{2\pi r^2}{\tan \alpha_1}}{\frac{2\pi r^2}{\tan \alpha_2}} = \frac{\tan \alpha_2}{\tan \alpha_1}$$

Therefore, for instance, the area ratio of the 5°- and 15°-nozzle is

$$\frac{A_1}{A_2} = \frac{\tan \alpha_2}{\tan \alpha_1} = \frac{\tan 15^\circ}{\tan 5^\circ} \approx 3$$

Appendix D

Images



Image 1. Equipment from left: Piston system, pressure sensor and datalogger.



Image 2. A close-up view on the piston.



Image 3. Detailed view on the piston system and an engine in it.

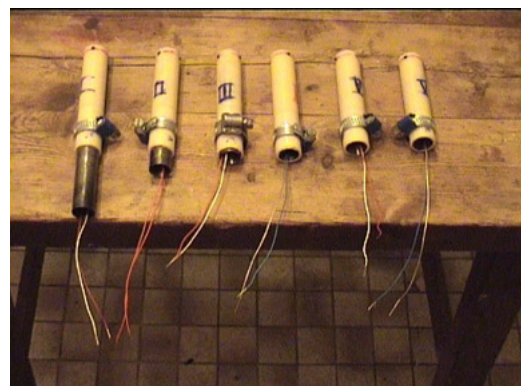


Image 4. A set of rockets. Leftmost an engine with a 5°-nozzle and rightmost an engine with a 45°- nozzle. Detonator wires are visible as well.